The utilization of boron nitride (BN) for granular L1$_0$-FePt HAMR media fabrication F

ⓘD Bing Zhou, ⓘD David E. Laughlin, and ⓘD Jian-gang (Jimmy) Zhu

COLLECTIONS

F   This paper was selected as Featured

View Online   Export Citation   CrossMark

ARTICLES YOU MAY BE INTERESTED IN

Microscopic metallic air-bridge arrays for connecting quantum devices
Applied Physics Letters 118, 162108 (2021); https://doi.org/10.1063/5.0045557

Room-temperature two-terminal magnetoresistance ratio reaching 0.1% in semiconductor-based lateral devices with L2$_1$-ordered Co$_2$MnSi
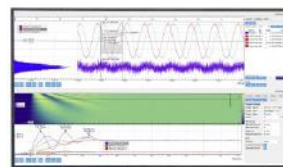Applied Physics Letters 118, 162404 (2021); https://doi.org/10.1063/5.0045233

Dispersive readout of reconfigurable ambipolar quantum dots in a silicon-on-insulator nanowire
Applied Physics Letters 118, 164002 (2021); https://doi.org/10.1063/5.0040259

The utilization of boron nitride (BN) for granular L1$_0$-FePt HAMR media fabrication

Bing Zhou,[1,2,a)] David E. Laughlin,[1,2,3] and Jian-gang (Jimmy) Zhu[1,2,3]

AFFILIATIONS

[1]Data Storage Systems Center, Carnegie Mellon University, Pittsburgh, Pennsylvania 15213, USA
[2]Materials Science and Engineering Department, Carnegie Mellon University, Pittsburgh, Pennsylvania 15213, USA
[3]Electrical and Computer Engineering Department, Carnegie Mellon University, Pittsburgh, Pennsylvania 15213, USA

[a)]Author to whom correspondence should be addressed: bingzhou@andrew.cmu.edu

ABSTRACT

In this experimental study, we present a dual-layer structure of FePt-boron nitride (BN)/FePt-SiO$_x$ granular media for the heat-assisted magnetic recording. The boron nitride (BN) was deposited together with FePt at 700 °C for the first 2.5 nm in the initial film growth. After the initial growth, SiO$_x$ was used to replace the BN to serve as the grain boundary material for the rest of film growth process. The transmission electron microscopy study on the fully grown FePt-BN/FePt-SiO$_x$ film shows well-isolated FePt grains that are fully encircled by the well-defined grain boundaries. The areal density of FePt grains is distinctively higher than that of the conventional granular FePt-C-based film at similar film thickness. The FePt-BN/FePt-SiO$_x$ bilayer granular media also demonstrate excellent magnetic properties, which are comparable to that of FePt-C-SiO$_x$ granular media in terms of the hysteresis characteristics.

Published under license by AIP Publishing. https://doi.org/10.1063/5.0045901

In granular L1$_0$-ordered FePt thin film media for the heat-assisted magnetic recording (HAMR), low thermal conductance materials separating neighboring magnetic grains are critical in facilitating a relatively high lateral thermal gradient during the recording processes. As a result, a microstructure with well-defined grain boundaries that fully encircle individual FePt grain is desirable to increase the data storage density capability. Moreover, since the signal-to-noise ratio (SNR) in recording performance is directly proportional to the grain areal density, it is essential to reduce the grain-to-grain pitch distance while maintaining the desirable thin film microstructure and the magnetic properties in the effort to increase the media areal density capability (ADC).

Granular FePt-C media with carbon as the sole grain boundary material has been considered to be successful in the past, because it results in a microstructure with isolated FePt grains that are fully encircled by the well-defined grain boundaries of C. Such media also shows excellent L1$_0$ ordering and magnetic properties.[1] However, as the push for higher grain areal density continues, it has been found that the grain areal density of FePt-C media on MgO underlayer (UL) is limited and it decreases with increasing deposition temperature.[2] Carbon in the grain boundaries does not seem to be able to constrain lateral growth and the aggregation of FePt grains due to its high mobility at elevated temperature.[2,3] Consequently, in FePt-C films, the FePt

grain size increases and the grain center-to-center pitch distance decreases with increasing magnetic layer thickness, which limits the grain areal density for relatively thicker films. Combined with the possible formation of a secondary layer of nontextured FePt grains often found in FePt-C media, growing the FePt grains of high height-to-diameter aspect ratio has proven to be challenging.

On the other hand, FePt-SiO$_x$ media with SiO$_x$ as the sole grain boundary material has shown good columnar structure with good chemical ordering and magnetic properties. However, it often results in interconnected worm-shaped FePt grains with disconnected grain boundaries.[4,5] This inadequate microstructure directly yields degraded recording performance with higher transition jitter noise.

In an attempt to take the advantages of both the C and SiO$_x$ while avoiding their shortfalls, FePt-C/FePt-SiO$_x$ multilayers have been investigated with FePt-C as the initial nucleation layer followed by the deposition of FePt-SiO$_x$ layer.[6,7] With this approach, FePt in the upper layer grows on the FePt grains of the lower layer while the SiO$_x$ grain boundaries grow on top of the C grain boundaries. The vertical alignment of the grain boundaries results in significantly improved granular microstructure for the FePt-SiO$_x$ layer on top, where FePt grains are fully encircled by the oxide grain boundaries. However, the grain areal density in initial FePt-C layer seemed to be limited, which determines the final grain-to-grain pitch distance in the full stack film structure.

More recent studies indicated that the limitation of initial FePt-C layer grain density is the result of the grain nucleation process of FePt-C on MgO underlayer.[2] In this study, boron nitride (BN) is used as the grain boundary material for the initial growth of FePt layer followed by FePt-SiO$_x$. The microstructure of the resulting bilayer thin film structure of FePt-BN/FePt-SiO$_x$ is analyzed using transmission electron microscopy (TEM). The texture and ordering of the resulting film characterized by X-ray diffraction (XRD) are reported with its magnetic hysteresis measurements.

All thin film samples were fabricated using AJA sputtering systems with a base pressure at than 8×10^{-9} Torr or lower. The initial buffer layer film stack Ta (5)|Cr (40) was deposited on Si substrates (the numbers in parentheses in nm). The Ta and Cr layers were DC sputtered at room temperature and 280 °C, respectively. The stack was subsequently annealed at 650 °C for 1 h in vacuum in order to promote the texture and grain size of the Cr buffer layer. After the sample cooled to room temperature, 8 nm of MgO was deposited on top of Cr layer using RF sputtering at 10 mTorr. The same film stack of Ta(5)|Cr(40)|MgO(8) was used for magnetic layer deposition throughout this paper, so it will be referred to as the underlayer or UL for simplicity in the later part of the paper unless otherwise stated. The substrate was then reheated to 700 °C, and a 0.5 nm pure FePt was deposited via DC sputtering on top of MgO. This layer will be referred to as M0 layer in this paper. Maintaining the substrate temperature above, a 2 nm FePt-38 vol. % BN layer was deposited on M0 layer with FePt deposited via DC sputtering and BN deposited via RF sputtering. BN target used in this paper was polycrystalline target with purity level >99.5%. Since the sputtering yield of BN is substantially lower than that of FePt, co-sputtering will not enable sufficient BN percentage in the resulting film layer. Maximum volume percentage of BN can be achieved via co-sputtering with FePt is 9 vol. %. Therefore, this 2 nm FePt-BN layer was realized by multiple repeats of alternative deposition of 2.2 Å FePt-9 vol. % BN (co-sputtered) and 1 Å BN (RF-sputtered). This magnetic layer will be referred to as M1 layer in this paper. The substrate was then cooled to 550 °C and maintained at this temperature for the deposition of the FePt-SiO$_x$ layer. A 4 nm FePt-35 vol. % SiO$_x$ was deposited on the M1 layer by co-sputtering FePt (DC sputtering) and SiO$_x$ (RF sputtering). The SiO$_x$ target used in this paper was polycrystalline target with purity level >99.999%. This layer will be referred to as the M2 layer in this paper. Table I shows the sputtering pressures used for all the layers along with their corresponding deposition rates. The entire film stack of Ta(5)|Cr(40)|MgO(8)|FePt(0.5)|FePt-BN(2)|FePt-SiO$_x$(4) was fabricated according to the above sequence without breaking the vacuum.

The crystalline texture and degree of chemical ordering of all samples were determined using X-ray diffraction (XRD) spectra using Cu K$_a$ radiation. The magnetic properties were analyzed using Quantum Design's Magnetic Property Measurement System (MPMS 3) with a maximum field of 7 T. The microstructure and atomic structure of the samples were evaluated using bright-field transmission electron microscopy (TEM) imaging, high-resolution-TEM imaging (HR-TEM), and scanning TEM-high angle annular dark field imaging (STEM-HAADF). The grain size and the grain center-to-center pitch distance were analyzed using the STEM-HAADF images of the samples and the imaging software for accuracy and consistency. For the grain center-to-center pitch distance analysis, the number of nearest neighboring grains was estimated to be 6 for each grain.

Figure 1(a) illustrates the cross-sectional schematic of the full film structure. Figure 1(b) shows the perpendicular and the in-plane hysteresis loops of the sample at room temperature with its XRD pattern shown in Fig. 1(c). A perpendicular coercivity of $H_{c,\perp} = 2.7$ T was obtained. The in-plane loop shows a small opening with a coercivity of $H_{C,//} = 0.32$ T and a normalized remanence magnetization $M_{r,///}/M_s = 0.08$, suggesting that the c-axis of FePt grains is predominantly perpendicular to the thin film plane. The perpendicular-to-in-plane remanence ratio, $M_{r,///}/M_{r,\perp} = 0.09$, is relatively small, suggesting only a minor in-plane component of FePt grains in the sample. The XRD pattern shows only (001) and (002) peaks from FePt, indicating a strong texture of the FePt grains. The integrated
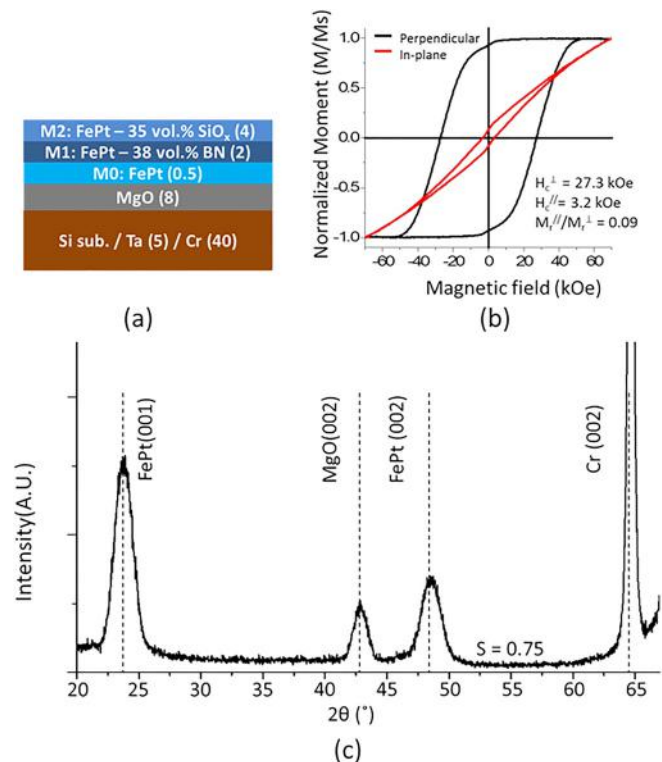
TABLE I. Deposition rates and pressures of all targets.

Targets	Deposition rates (Å/s)	Pressure (mTorr)
Ta	0.4	2
Cr	0.3	2
MgO	0.08	10
FePt	0.2	5
BN	0.02	5
SiO$_x$	0.11	5

FIG. 1. (a) Schematic of the thin film structure Ta(5)|Cr(40)|MgO(8)|FePt(0.5)|FePt-38 vol. % BN(2)|FePt-35 vol. % SiO$_x$(4) with its (b) magnetic hysteresis loops and (c) XRD pattern.

intensity ratio between FePt superlattice peak (001) and fundamental peak (002) (I_{001}/I_{002}) is about 2.1, suggesting good chemical ordering of FePt grains. Taking into account the integrated intensity ratio between FePt (001) and (002) (I_{001}/I_{002}), finite film thickness and other corrections, the order parameter of the film sample calculated is $S = 0.75$.[8]

Figure 2(a) shows the plane-view HAADF image and (b) the cross section HRTEM image of the full-stack film structure. In the plane-view HAADF image, the neighboring FePt grains (bright) are almost completely isolated by nonmetallic grain boundaries (dark) without adjacent grains appearing to be connected (one may still find only a few connected grains in the image although there are less than a handful). The cross section HRTEM image shows that the columnar grains have the same grain diameter over the entire 6.5 nm magnetic layer stack. The FePt of M0 + M1 + M2 and the grain boundaries of M1 + M2 layer are perfectly aligned without any sign of disruption at the M1 and M2 interface. The grain size distribution profile and the pitch distance distribution profile calculated from this image and other images of the same sample are shown in Figs. 2(c) and 2(d), respectively. The distribution profiles show a mean grain size of 6.4 nm and a mean pitch distance of 8.4 nm. More importantly, the grain size distribution profile shows clear single-modal, which is quite different from the typical bimodal grain size distribution shown in the FePt-C film.[3]

The significance of the full film results shown above will be discussed first. It can be observed that when FePt-SiO$_x$ is deposited on top of FePt-BN (2 nm) layer, virtually all FePt grains (with few exceptions) are completely encircled by well-defined oxide grain boundaries without the adjacent grains being connected. This result is in startling contrast to the microstructure of a single layer of FePt-SiO$_x$ directly deposited on MgO. In the case of MgO/FePt-SiO$_x$, the oxide grain boundaries often only partially encircle the FePt grains and consequently a large percentage of adjacent FePt grains become connected through oxide-missing gaps along grain boundaries to form elongated

worm-shaped grains.[4] Although a few grains can still be found connected in the HAADF image shown in Fig. 2, their percentage is significantly lowered to a single digit. The FePt-BN layer underneath the FePt-SiO$_x$ layer is apparently playing an important role in creating/facilitating the observed granular isolated microstructure. The almost perfect grain boundary alignment at the M1/M2 interface in the perpendicular direction reaffirms this suggestion.

Second, the grain size distribution profile of the full film structure shows only a single modal distribution. This is also a significant improvement over a single layer of FePt-C directly deposited on MgO. In the case of MgO/FePt-C, the bimodal distribution of the grain size often occurs with the second modal being at a relatively smaller distribution of the grain size centering at around 2–3 nm.[3,9,10] The existence of a second modal grain size distribution in FePt-C/MgO has been attributed to the continuous nucleation of FePt grains on the MgO throughout the film growth process. Our previous study has shown that FePt atoms can easily penetrate through continuous carbon grain boundaries to land on MgO even at later stage of the film growth during elevated-temperature deposition.[3] The BN and SiO$_x$ grain boundaries seem to prevent the continuous nucleation of FePt on MgO as the bimodal grain size distribution is completely absent. An experimental modeling study to compare the stability of C grain boundaries with BN grain boundaries at elevated temperature has been done, and the detailed results can be found in the supplementary material.

Since the FePt-BN M1 layer has significant impact on the microstructure of the full stack media, the microstructure of M0 + M1 layer prior to the deposition of FePt-SiO$_x$ M2 layer was studied. Figure 3(a) shows the in-plane HAADF image of the film stack FePt(0.5)/FePt-BN(2) on the same prefabricated underlayer structure as the full stack film with the FePt grain pitch distance shown in the inset. Moreover, the thickness of FePt-BN M1 layer was doubled to 4 nm to investigate the microstructure change and the in-plane HAADF image is shown in Fig. 3(b) with the FePt grain pitch distance shown in the inset.
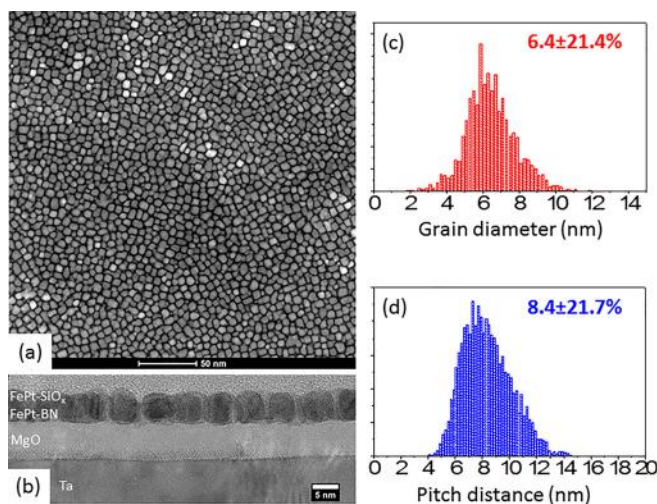

FIG. 2. (a) In-plane HAADF image and (b) cross section TEM image of the film stack Ta(5)|Cr(40)|MgO(8)|FePt(0.5)|FePt-38 vol. %BN(2)|FePt-35 vol. % SiO$_x$(4) with its (c) grain size distribution and (d) grain center-to-center pitch distance distribution.
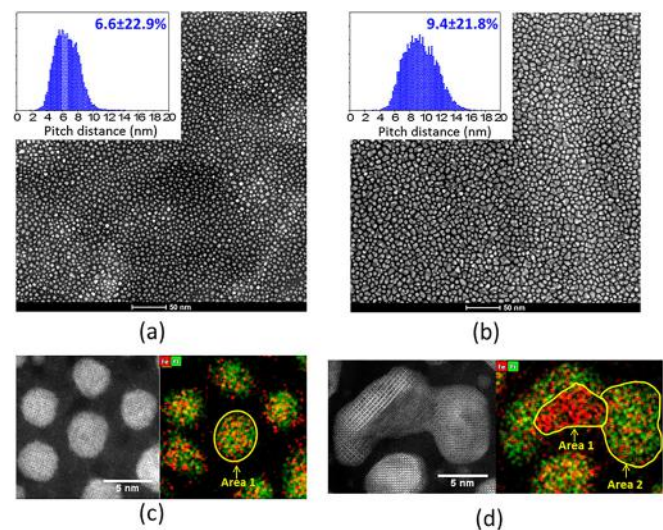

FIG. 3. In-plane HAADF images of the film stack FePt (0.5)/FePt-BN (n) on an MgO underlayer, where n = 2 (a) and 4 nm (b). The insets are their corresponding grain center-to-center pitch distance distribution; HAADF image and EDS mapping of Fe and Pt from (c) FePt (0.5)|FePt-BN (2) and (d) FePt (0.5)|FePt-BN (4).

Figures 3(c) and 3(d) show the energy dispersive x-ray spectroscopy (EDS) mapping of Fe (red) and Pt (green) from a representative area of the samples of 2 nm and 4 nm M1 layer, respectively. It can be observed that Fe and Pt atoms are generally evenly distributed in the FePt grains in the case of 2 nm M1 layer, shown in Fig. 3(c), and the chemical composition of area 1 shows 49 at. % Fe and 51 at. % Pt, which is near equal atomic percentage (correct for $L1_0$ structure). In contrast, with Fig. 3(d), it can be observed from the EDS mapping that area 1 is dominated in red (Fe) compared to the rest of the grain. The chemical composition from area 1 in Fig. 3(d) shows 70 at. % Fe and 30 at. % Pt, whereas that from area 2 shows 44 at. % Fe and 56 at. % Pt. It can be observed that (i) the FePt grains are well dispersed in the case of the 2 nm FePt-BN film and the distance between neighboring grains appear to be quite uniform although there exists some very small grains; (ii) the non-FePt area appears to be greater than 38%, which is the volume percentage of BN added, indicating that the FePt grains in FePt-BN layer grow on top of the FePt nucleation sites created by 0.5 nm FePt (M0 layer) and the height of BN grain boundaries in the area between adjacent FePt grains is likely to be lower than FePt grain height at this stage; (iii) the grain size and the grain pitch distance increase when the thickness of FePt-BN M1 layer increases from 2 nm to 4 nm. The increase in pitch distance is likely resulted from the interconnection of the adjacent FePt grains as shown in Fig. 3(d). The interconnected region bridging the two adjacent grains is likely grown over BN such that it is unlikely to be $L1_0$-ordered and the corresponding EDS elementary mapping shows the bridging region likely to be Fe-rich. Hence, an adequate thickness of FePt-BN is important for providing the proper grain microstructure "template" for the growth of FePt-SiO$_x$ layer on top.

It is worth mentioning that our choice of depositing a 0.5 nm pure FePt layer as the initial nucleation layer on the MgO is based on the understanding in a study by Suzuki *et al.* in which they showed that the FePt grain density is higher in the nucleation stage when pure FePt is directly deposited on the MgO.[2] This 0.5 nm FePt layer does seem to serve well as a nucleation layer in this study as the FePt grains in the subsequent FePt-BN layer all seem to have grown on top of the FePt grains in M0 layer. A comparison study of the grain pitch distance between 0.5 nm FePt and 0.5 nm FePt-38 vol. % BN has been performed, and the results are included in the supplementary material.

By comparing the mean grain pitch distance of the microstructure after M1 and M2 layer, an increase from 6.6 nm to 8.4 nm can be noted. In fact, the mean grain pitch distance is about 5.5 nm after the 0.5 nm pure FePt layer (M0), 6.6 nm after the 2 nm FePt-BN layer (M1), and 8.4 nm after the 4 nm FePt-SiO$_x$ layer (M2). The increase in the grain pitch distance at each of the stages above is likely due to the discontinuation of the growth of the small FePt grains. Very small or short FePt grains have higher possibilities to be covered by BN during the deposition of the FePt-BN layer. Such discontinuation of the small or short FePt grains are more likely to happen if they are situated closely in between comparably larger grains. The disappearance of the small grains obviously will lead to the increase in pitch distance in the next layer, as this phenomenon is illustrated by the cartoon of the grain growth in Fig. 4. We also believe the same phenomenon happens at the interface of M1 and M2, yielding a further increase in the grain pitch distance. Since the small or short grains shadowed by relatively large neighboring grains are more likely to discontinue growing, it is
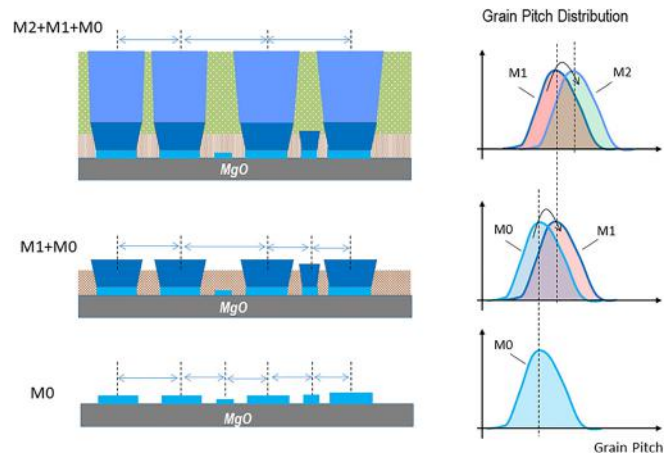

FIG. 4. Illustration of the likely mechanism leading to grain pitch increase at subsequent film growth stages.

possible that some of these small grains are not observable in the TEM image at the later stages; consequently, the observed grain pitch distance increases from M0 layer to M2 layer.

With the above understanding, one can see that the nucleation density of initial FePt is not persevered due to the growth discontinuation of some of the grains with smaller sizes and lower heights. The uniformity of the size and height of the FePt grains in the initial film growth, therefore, is important for preserving the initial nucleation density. In practice, one may not be able to avoid such distribution and a higher initial nucleation density may still be important for achieving a higher grain density in the final film stack as the case shown here. Nonetheless, a more uniform size and height distribution can lead to the final grain pitch distribution closer to the initial grain nucleation density.

In summary, we have fabricated FePt/FePt-BN/FePt-SiO$_x$ granular thin film HAMR media with 0.5 nm pure FePt layer as the initial nucleation layer followed by a 2 nm FePt-BN layer to serve as the template layer for the final growth of the FePt-SiO$_x$ layer. This film stack enables excellent granular microstructure in the FePt-SiO$_x$ layer with oxide grain boundaries completely encircling FePt grains with very few interconnected grains caused by the coalescence of adjacent FePt grains in the FePt-SiO$_x$ layer. The SiO$_x$ grain boundaries on top well aligned with the BN grain boundaries underneath enabling the columnar growth of FePt grains without any sign of disruption at the interface between FePt-BN and FePt-SiO$_x$. The magnetic characteristics appear to be adequate, although more optimization is needed. The grain size of the full stack films clearly shows a single modal grain size distribution with mean grain size of 6.4 nm and mean pitch distance of 8.4 nm.

See the supplementary material for more experimental details.

DATA AVAILABILITY

The data that support the findings of this study are available within the article and its supplementary material.

REFERENCES

[1] A. Perumal, Y. K. Takahashi, and K. Hono, Appl. Phys. Express **1**, 101301 (2008).

[2] I. Suzuki, J. Wang, Y. K. Takahashi, and K. Hono, J. Magn. Magn. Mater. **500**, 166418 (2020).

[3] B. Zhou, B. S. D. C. S. Varaprasad, E. Zhang, D. E. Laughlin, and J. G. Zhu, IEEE Trans. Magn. **54**, 3201104 (2018).

[4] H. Ho, E. Yang, D. E. Laughlin, and J. G. Zhu, Appl. Phys. Lett. **102**, 112411 (2013).

[5] T. O. Seki, Y. K. Takahashi, and K. Hono, J. Appl. Phys. **103**, 023910 (2008).

[6] B. S. D. C. S. Varaprasad, M. Chen, Y. K. Takahashi, and K. Hono, IEEE Trans. Magn. **49**, 718 (2013).

[7] L. Zhang, L. Liu, K. Hayasaka, and S. Ishio, J. Alloys Compd. **651**, 389 (2015).

[8] E. Yang, D. E. Laughlin, and J. Zhu, IEEE Trans. Magn. **48**, 7 (2012).

[9] D. Weller, O. Mosendz, G. Parker, S. Pisana, and T. S. Santos, Phys. Status Solidi A **210**, 1245 (2013).

[10] S. Wicht, V. Neu, L. Schultz, D. Weller, O. Mosendz, G. Parker, S. Pisana, and B. Rellinghaus, J. Appl. Phys. **114**, 063906 (2013).